energies

MDPI

Article

Effects of Overnight Oxidation on Perovskite Solar Cells with Co(III)TFSI Co-Doped Spiro-OMeTAD

Laxmi Nakka [1,2], Armin Gerhard Aberle [1,2] and Fen Lin [1,*]

[1] Solar Energy Research Institute of Singapore (SERIS), National University of Singapore, Singapore 117574, Singapore
[2] Department of Electrical and Computer Engineering, National University of Singapore, Singapore 117583, Singapore
* Correspondence: lin.fen@nus.edu.sg

Abstract: Metal-halide perovskite solar cells (PSCs) have achieved remarkable power conversion efficiencies in recent years, and spiro-OMeTAD plays a significant role as a hole transport material in PSCs with record efficiencies. However, further studies and systematic experimental procedures on doped spiro-OMeTAD are required to enable a reliable process for potential commercialization. In particular, the effect of the prolonged oxidation of Co(III)TFSI co-doped spiro-OMeTAD has been one of the unanswered topics in PSC research. In this work, we investigate the influence of overnight oxidation on the performance of PSCs with Co(III)TFSI co-doped spiro-OMeTAD. Co-doping spiro-OMeTAD with Co(III) complexes instantly oxidizes spiro-OMeTAD, leading to an improvement in power conversion efficiency (PCE) from 13.1% (LiTFSI-doped spiro-OMeTAD) to 17.6% (LiTFSI + Co(III)TFSI-doped spiro-OMeTAD). It is found that PSCs with spiro-OMeTAD co-doped with Co(III)TFSI without overnight oxidation could retain around 90% of the efficiency under maximum power point tracking at 1-sun illumination for 3000 min, whereas the efficiencies drop by more than 30% when Co(III)TFSI co-doped spiro-OMeTAD is exposed to overnight oxidation. Hence, it is important to inhibit the unnecessary overnight oxidation of Co(III)TFSI co-doped spiro-OMeTAD so as to save excess fabrication time and overcome the poor stability issues.

Keywords: spiro-OMeTAD; doping; oxidation; perovskite solar cell

Citation: Nakka, L.; Aberle, A.G.; Lin, F. Effects of Overnight Oxidation on Perovskite Solar Cells with Co(III)TFSI Co-Doped Spiro-OMeTAD. *Energies* **2023**, *16*, 354. https://doi.org/10.3390/en16010354

Academic Editor: Adalgisa Sinicropi

Received: 15 November 2022
Revised: 23 December 2022
Accepted: 24 December 2022
Published: 28 December 2022

1. Introduction

Organic–inorganic metal halide perovskite solar cells (PSCs) have experienced very rapid development in recent years, with laboratory device efficiencies improving from 3.8% in 2009 [1] to an impressive 25.7% in 2022 [2]. Interface engineering and the synthesis of small molecules as additives and donors are the popular methods to improve the efficiency of organic solar cells [3–7]. In a perovskite solar cell, the hole transport material (HTM) is responsible for efficient hole extraction and facilitating faster hole transport [8,9]. Therefore, many organic and inorganic HTMs have emerged in the last decade and vibrant research is ongoing in the perovskite community for investigating the proper choice of HTMs [10–13]. Among several existing HTMs, 2,2′,7,7′-tetrakis[N,N-di(4-methoxyphenyl)amino]-9-9′-spirobifluorene (spiro-OMeTAD) is considered the most promising HTM due to its amorphous nature, solution processability, deep HOMO energy level and excellent thermal stability [14,15]. To achieve highly efficient perovskite solar cells (PSCs) using spiro-OMeTAD as an HTM, it is a common practice to chemically dope spiro-OMeTAD with lithium-bis(trifluoromethanesulfonyl)imide (LiTFSI) and 4-tert-butylpyridine (tBP) to improve the mobility and facilitate efficient hole transport. Nevertheless, experimental studies have shown that LiTFSI is an efficient dopant in the presence of oxygen, and it is a proven fact that the oxidation mechanism of spiro-OMeTAD depends on spectrum illumination or exposure to air [16,17]. Typically, the diffusion rate of oxygen in the spiro-OMeTAD film is too slow and the freshly fabricated LiTFSI-doped

spiro-OMeTAD films have to be exposed to oxygen for several hours to oxidize spiro-OMeTAD. This process is time-intensive, which not only imposes a serious limitation on the process duration but also causes the device to degrade more rapidly due to the hygroscopic nature of LiTFSI [18–20]. A critical understanding of the time-dependent oxidation behavior of spiro-OMeTAD is important. Dopants with a higher redox potential in comparison with the first oxidation potential of spiro-OMeTAD can readily oxidize the HTM [21–23]. For example, tris(2-(1H-pyrazol-1-yl) pyridine) cobalt(III) (FK209) or simply Co(III)TFSI can be used to co-dope spiro-OMeTAD to enhance the hole mobility and the device performance without the requirement for overnight oxidation [22]. However, this theoretical concept has not been proven in the literature and the reasons for the same have not been investigated with an experimental study. Moreover, it has been observed from the literature that researchers have exposed Co(III)TFSI co-doped spiro-OMeTAD to air with varied exposure times, and there was no significant improvement in the power conversion efficiency (PCE) of the perovskite solar cell in these reports [24–26]. In addition, the effect of stability on overnight oxidation has not yet been studied.

In this work, systematic experimental studies are carried out to demonstrate the effects of overnight oxidation on spiro-OMeTAD doped with (a) LiTFSI and (b) LiTFSI + Co(III)TFSI. They are termed LiTFSI-doped spiro-OMeTAD and Co(III)TFSI co-doped spiro-OMeTAD, respectively, throughout the paper. Experimental characterizations confirm that Co(III)TFSI co-doped spiro-OMeTAD does not show any time-dependent oxidation behavior as opposed to LiTFSI-doped spiro-OMeTAD. Most importantly, PSCs using Co(III)TFSI-doped spiro-OMeTAD without overnight oxidation have shown higher stability compared to Co(III)TFSI-doped spiro-OMeTAD without overnight oxidation.

2. Experimental Section

2.1. Materials

The patterned indium tin oxide (ITO)-coated glass substrates (sheet resistance 15 Ω-sq^{-1}, thickness 200 nm) were purchased from Yingkou Shangneng Photoelectric Material Co., Ltd., Yingkou, China. The perovskite precursor chemicals lead iodide (PbI_2) and methyl ammonium iodide (MAI) were purchased from TCI chemicals, Tokyo, Japan. The HTM 2,2′,7,7′-tetrakis[N,N-di(4-methoxyphenyl)amino]-9-9′-spirobifluorene (spiro-OMeTAD), the dopants lithium-bis(trifluoromethanesulfonyl)imide (LiTFSI), 4-tert-butylpyridine (tBP), tris(2-(1H-pyrazol-1-yl)pyridine), cobalt(III) (FK209), acetonitrile (ACN), dimethylformamide (DMF), dimethyl sulfoxide (DMSO), chlorobenzene (CB) and toluene (anhydrous) were all purchased from Sigma-Aldrich, St. Louis, MO, USA. SnO_2 solution (15% in H_2O colloidal dispersion liquid) was purchased from Alfa Aesar, Haverhill, MA, USA. All reagents were used without any purification.

2.2. Solution Preparation

The SnO_2 solution was prepared by mixing the SnO_2 nanoparticles in distilled water (DI) water in a ratio of 1:4 and was then ultrasonically treated for 30 min. The perovskite precursor solution was prepared by mixing 461 mg of PbI_2 and 159 mg of MAI in a 1 mL mixture of dimethylformamide (DMF) and dimethyl sulfoxide (DMSO) solvents in a 10:1 volume ratio. An amount of 72.3 mg of pristine spiro-OMeTAD was doped with 17.5 µL of Li-TFSI and 28.5 µL of tBP, which were dissolved in 1 mL of chlorobenzene. Further, cobalt co-doped spiro-OMeTAD solution was prepared by adding 8 µL of Co(III)TFSI to LiTFSI + tBP-doped spiro-OMeTAD solution.

2.3. Device Fabrication

The perovskite solar cells used in this research were fabricated by a sequential deposition process. Before depositing the films, the ITO-coated glass substrate was sonication-cleaned in cleaning solution (2% Hellmanex solution diluted in DI water in the ratio 1:4), acetone, and isopropanol (IPA) for 15 min each, followed by UV ozone treatment for 20 min. SnO_2 was then spin-coated at 4000 rpm for 40 s, followed by annealing at 150 °C for 30 min

in air. The sample was transferred to a nitrogen-filled glovebox with H_2O and O_2 concentrations of <0.01 ppm. The perovskite film was deposited in a two-step process. Firstly, the $MAPbI_3$ perovskite precursor solution was deposited at 4000 rpm for 30 s. During the second step, 200 µL of toluene was dynamically dripped onto the substrates at 7 s after the spinning started. The perovskite film was then annealed at 100 °C for 10 min, followed by the deposition of spiro-OMeTAD at 4000 rpm for 40 s. Finally, the silver electrode of a thickness of 200 nm was deposited on the spiro-OMeTAD layer by thermal evaporation.

Two pairs of $MAPbI_3$-based perovskite solar cells with spiro-OMeTAD as an HTM with an active area of 0.1 cm^2 were fabricated in this work, one pair using LiTFSI as dopants in spiro-OMeTAD and the other pair using LiTFSI + Co(III)TFSI as dopants in spiro-OMeTAD. All devices were studied under two conditions, namely without overnight oxidation and with overnight oxidation for 18 h. The oxidation process takes place before the deposition of the metal electrode. The samples with overnight oxidation were kept in the dark inside the oxidation chamber.

2.4. Measurements and Characterizations

The current density–voltage (J–V) characterization was performed using a Keithley 2400 source meter (class A/B Xenon, 550 W solar simulator, Abet Tech, Milford, CT, USA) under one-sun illumination (AM 1.5, 100 $mWcm^{-2}$) in a nitrogen-purged glovebox. Before the J–V measurements, the solar simulator was powered on, stabilized for 30 min, and a mono-crystalline silicon reference cell was used for calibration. The absorption spectra of the films were obtained using a UV-VIS-NIR Spectrophotometer (Cary7000, Agilent, Singapore). Steady-state photoluminescence (PL) and time-resolved photoluminescence (TRPL) spectra measurements were conducted using a Time-resolved Fluorescence Spectrometer (FluoTime 300, Picoquant, Berlin, Germany) with an excitation wavelength intensity of 520 nm. Contact angle measurements were performed with a Tensiometer using diiodomethane (DIM). X-ray diffraction (XRD) measurements were carried out using an Aeris XRD System (Malvern Panalytical, Malvern, UK). The device stability measurements were performed using a Keithley 2400 source meter, under continuous 1-sun illumination in a nitrogen-purged glovebox.

3. Results and Discussion

The current density–voltage characteristics (J–V) of the perovskite solar cells were measured under AM 1.5 G (100 mW cm^{-2}) illumination. The J–V curves of the fabricated perovskite solar cells with LiTFSI-doped spiro-OMeTAD and Co(III)TFSI co-doped spiro-OMeTAD with and without overnight oxidation are shown in Figure 1a and the photovoltaic parameters are summarized in Table 1. The power conservation efficiency (PCE) and short circuit current density (J_{SC}) of the device with LiTFSI-doped spiro-OMeTAD are only 9.2% and 14.8 mA/cm^2, respectively, without overnight oxidation. Spiro-OMeTAD has to generate free radical cations in order to improve its conductivity and thereby the J_{SC} of the perovskite solar cell. This is possible only under overnight oxidation, as per the reaction shown in Equation (1). When the LiTFSI-doped spiro-OMeTAD film was subjected to overnight oxidation, the J_{SC} improved remarkably from 14.8 to 21.6 mA/cm^2. On the other hand, no significant variations in J_{SC} and PCE were observed for the devices based on Co(III)TFSI co-doped spiro-OMeTAD as HTM for the cases of with and without overnight oxidation. This is due to the instant oxidation mechanism of spiro-OMeTAD in the presence of cobalt complexes, as per the reaction in Equation (2). This leads to an increased power conversion efficiency of >17%, indicating that the performance of Co(III)TFSI co-doped spiro-OMeTAD is superior to the LiTFSI-doped spiro-OMeTAD.

$$\text{Spiro} - \text{OMeTAD} + O_2 + \text{LiTFSI} \xrightarrow[(380-450\,\text{nm})]{h\nu} \text{Spiro} - \text{OMeTAD}\ \text{TFSI}^+\ \text{TFSI}^- + \text{Li}_x\text{O}_y \quad (1)$$

$$\text{Spiro} - \text{OMeTAD} + O_2 + \text{LiTFSI} + \text{Co(III)TFSI} \xrightarrow[(380-450\,\text{nm})]{h\nu} \text{Spiro} - \text{OMeTAD}\ \text{TFSI}^+\ \text{TFSI}^- + \text{Co(II)} + \text{Li}_x\text{O}_y \quad (2)$$

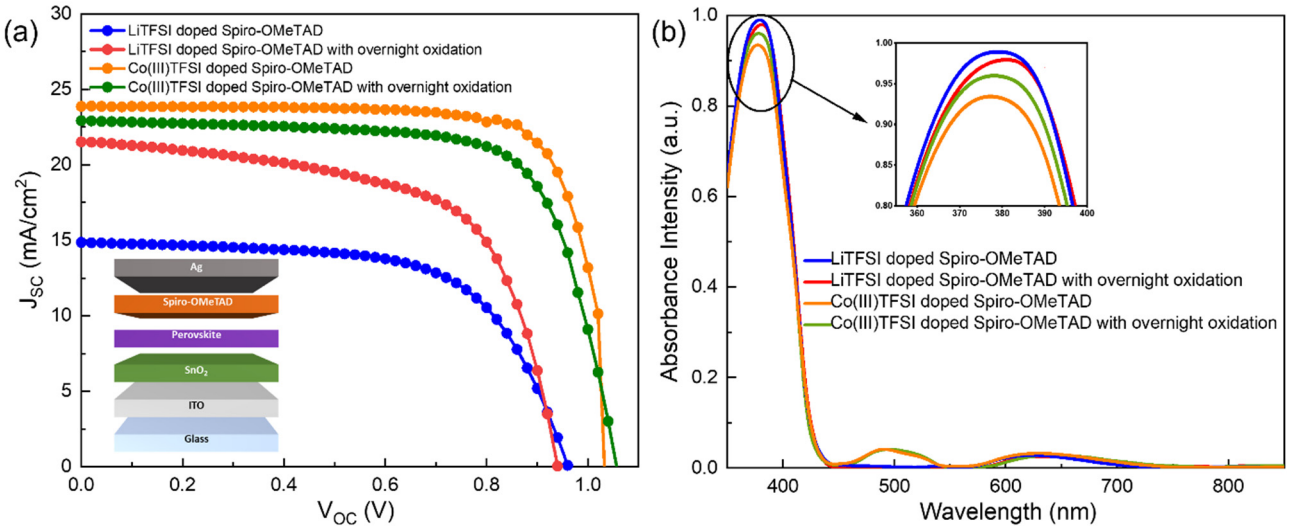

Figure 1. (**a**) J–V Characteristics of the perovskite solar cells with LiTFSI-doped spiro-OMeTAD and Co(III)TFSI co-doped spiro-OMeTAD under different oxidation conditions. The device structure of the fabricated n-i-p configuration perovskite solar cell is also shown in the figure, and (**b**) UV-Vis absorption spectra of doped spiro-OMeTAD films under different oxidation conditions. The figure in the inset shows the magnified portion of the UV-Vis spectra between 350 and 400 nm to clearly indicate the variation in the peak intensities.

Table 1. Summary of the photovoltaic parameters of the perovskite solar cells employing LiTFSI-doped spiro-OMeTAD and Co(III)TFSI co-doped spiro-OMeTAD with and without overnight oxidation.

Device	V_{OC} (V)	J_{SC} (mA/cm^2)	FF (%)	PCE (%)
PSC with LiTFSI-doped spiro-OMeTAD	965	14.8	64.5	9.2
PSC with LiTFSI-doped spiro-OMeTAD with overnight oxidation	954	21.6	62.6	12.9
PSC with Co(III)TFSI co-doped spiro-OMeTAD	1002	23.8	72.6	17.9
PSC with Co(III)TFSI co-doped spiro-OMeTAD with overnight oxidation	1006	22.8	73.0	17.6

To elucidate the reasons for this enhanced performance, UV-Vis spectroscopy was performed on these two pairs of devices and the results are shown in Figure 1b. An absorption peak is observed at 380 nm for all devices. In particular, as shown in the inset of Figure 1b, it is observed that the primary absorption peak of Co(III)TFSI co-doped spiro-OMeTAD is lower than that of LiTFSI-doped spiro-OMeTAD. This shows that the Co(III)TFSI co-doped spiro-OMeTAD is more transparent to the short-wavelength incident light, which may relatively increase the number of short-wavelength photons reaching the perovskite. The second absorption peak at 460–540 nm is observed only in the case of Co(III)TFSI co-doped spiro-OMeTAD. This indicates the occurrence of an instant oxidation process and the formation of spiro-OMeTAD+ radical ions which have a typical absorption peak around 500 nm [22]. In addition to these observations, it is clearly evident that the absorption peak at 500 nm has similar intensities for Co(III)TFSI co-doped spiro-OMeTAD regardless of oxidation conditions, which is not the case for LiTFSI-doped spiro-OMeTAD.

Steady-state photoluminescence (PL) is performed on the perovskite, perovskite/LiTFSI-doped spiro-OMeTAD, and perovskite/Co(III)TFSI co-doped spiro-OMeTAD films under different oxidation conditions to observe carrier generation and carrier extraction. Firstly, photoluminescence is measured on the perovskite layer deposited on the glass, as shown in Figure 2a, and a PL peak is obtained at 770 nm. Further on, when LiTFSI-doped spiro-OMeTAD is deposited on the perovskite, the PL peak is quenched. As a comparison, when the measurement is repeated by depositing Co(III)TFSI-co-doped spiro-OMeTAD on the perovskite, it is observed that the PL peak is significantly quenched by 90% compared to the initial perovskite layer. PL quenching is an indication of an enhanced hole extraction rate and efficient hole transfer between the perovskite and Co(III)TFSI co-doped spiro-OMeTAD [27]. The quenched PL peak shows that the mobile charge carriers generated by light illumination are separated and the holes are transferred efficiently by the doped spiro-OMeTAD. It is interesting to note that, regardless of oxidation conditions, the poor performance of LiTFSI-doped spiro-OMeTAD-based PSCs is consistent with the corresponding poor PL quenching. In addition, a blue shift of about 10 nm in the PL peak is observed after depositing Co(III)TFSI co-doped spiro-OMeTAD onto the perovskite, which is a further indication that cobalt complexes facilitate enhanced hole extraction and the generation of excess charge carriers [28]. Lastly, to study the crystal defects, we extracted the full-width half maximum (FWHM) of the steady-state PL spectra. As shown in Figure 2a, the FWHM of Co(III)TFSI co-doped spiro-OMeTAD is smaller than that of the LiTFSI-doped spiro-OMeTAD, indicating that the interface between perovskite and Co(III)TFSI co-doped spiro-OMeTAD has less defect density [29] and provides better passivation compared to LiTFSI-doped spiro-OMeTAD films. Moreover, as the defect density at the perovskite/HTM interface affects the V_{OC} [30], it is noteworthy to observe that the devices with Co(III)TFSI co-doped spiro-OMeTAD reported higher V_{OC} than the devices with LiTFSI-doped spiro-OMeTAD (Table 1). As a result of this analysis, it can be confirmed that Co(III)TFSI co-doped spiro-OMeTAD does not require overnight oxidation. Noticeably, the PL peaks have similar intensities for Co(III)TFSI co-doped spiro-OMeTAD regardless of oxidation conditions.

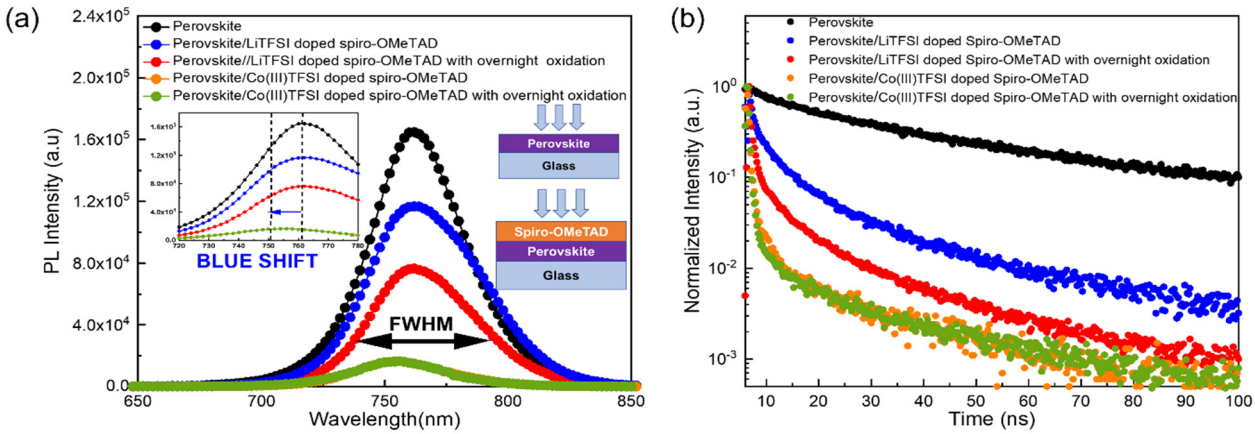

Figure 2. Photoluminescence spectra of the perovskite, perovskite coated with LiTFSI-doped spiro-OMeTAD, and perovskite coated with Co(III)TFSI co-doped spiro-OMeTAD on a glass substrate. The doped spiro-OMeTAD films are subjected to different oxidation conditions. (**a**) Steady-state PL. The inset shows the enlarged spectrum of PL between 720 and 780 nm to depict the blue shift. (**b**) TRPL.

In addition, transient photoluminescence (TRPL) measurements were also conducted to further study the carrier lifetimes (τ) for all cases of doped spiro-OMeTAD films deposited on the perovskite layer. As shown in Figure 2b, the obtained TRPL spectra are fitted using a biexponential decay model to obtain the lifetime values, and the results are summarized in Table 2. As can be seen, the single-layer perovskite film deposited on a glass substrate exhibits the highest lifetime of 1957 ns. When the LiTFSI-doped spiro-OMeTAD film is coated on top of the perovskite, it is observed that the lifetimes significantly reduce

to 284 ns and 145 ns, respectively, for the cases of with and without overnight oxidation. In comparison, for the perovskite films coated with Co(III)TFSI co-doped spiro-OMeTAD, the lifetime is further shortened to 98 ns and 102 ns, respectively, for the cases with and without overnight oxidation. This greater degree of lifetime reduction is also an indication that Co(III)TFSI co-doped spiro-OMeTAD results in faster hole extraction and more efficient hole transfer, which leads to higher hole mobility in the HTM. This is in good agreement with the superior device performance of Co(III)TFSI co-doped spiro-OMeTAD-based PSCs compared to devices using LiTFSI-doped spiro-OMeTAD. It is again noted that there is no significant lifetime difference in the cases of Co(III)TFSI co-doped spiro-OMeTAD with and without overnight oxidation.

Table 2. Carrier lifetimes extracted from the TRPL spectra for LiTFSI-doped spiro-OMeTAD and Co(III)TFSI co-doped spiro-OMeTAD under different oxidation conditions.

Film	Extracted Lifetime τ (ns)
Perovskite	1957
Perovskite/LiTFSI-doped spiro-OMeTAD	284
Perovskite/LiTFSI-doped spiro-OMeTAD with overnight oxidation	145
Perovskite/Co(III)TFSI co-doped spiro-OMeTAD	98

The crystalline structures of perovskite and the associated crystal defects due to doped spiro-OMeTAD films can be analyzed using X-ray diffraction. This is particularly useful to investigate whether the presence of Co(III)TFSI causes higher-order defects in the perovskite. Figure 3 shows the XRD results of the perovskite layers coated with LiTFSI and Co(III)TFSI co-doped spiro-OMeTAD. As shown in the figure, when perovskite layers are analyzed with doped HTM coatings without overnight oxidation, four XRD peaks are observed at 13.9°, 20.56°, 27.8°, and 41.61°, representing the perovskite peaks for (110), (120), (220), and (330) crystal planes, respectively. The first peak at 13.9° is the perovskite phase, and it is an indication of perovskite crystal purity [31]. For the cases without overnight oxidation, no significant difference in diffraction peaks and intensity is observed between perovskite layers coated with LiTFSI-doped spiro-OMeTAD or Co(III)TFSI co-doped spiro-OMeTAD. However, for the case with overnight oxidation, a strong diffraction peak at 11.2°, indicating hydrated MAPbI ($MAPbI.H_2O$), is observed for perovskite layers coated with LiTFSI-doped spiro-OMeTAD. This lower angle diffraction peak occurs due to the deformation of perovskite crystal, which is clear evidence of moisture ingress into the perovskite due to the prolonged oxidation of LiTFSI dopants. Surprisingly, this diffraction is also visible in the case of Co(III)TFSI co-doped spiro-OMeTAD with overnight oxidation. Hence, exposing Co(III)TFSI co-doped spiro-OMeTAD to oxygen for prolonged intervals negatively impacts the active perovskite layer. In addition to this strong peak, a weak peak at 12.54° is also observed, which is attributed to the Pb-based defects in the perovskite, and it is seen only in the case of LiTFSI-doped spiro-OMeTAD with overnight oxidation. The reaction of lead with iodine is triggered in the presence of LiTFSI+tBP salts, and this undesirable effect can be mitigated by reducing the concentration of tBP in the spiro-OMeTAD solution. The addition of Co(III)TFSI alters the concentration of tBP and hence no such peak is observed in the case of Co(III)TFSI co-doped spiro-OMeTAD (both with and without oxidation). Although the peak at 11.2° also exists in the case of perovskite coated with Co(III)TFSI co-doped spiro-OMeTAD with overnight oxidation, the intensity of such a peak is several magnitudes lower compared to the LiTFSI-doped spiro-OMeTAD with overnight oxidation. This analysis shows that Co(III)TFSI is a preferable co-dopant for spiro-OMeTAD (especially without overnight oxidation) to preserve the chemical structure of perovskite and improve the device performance.

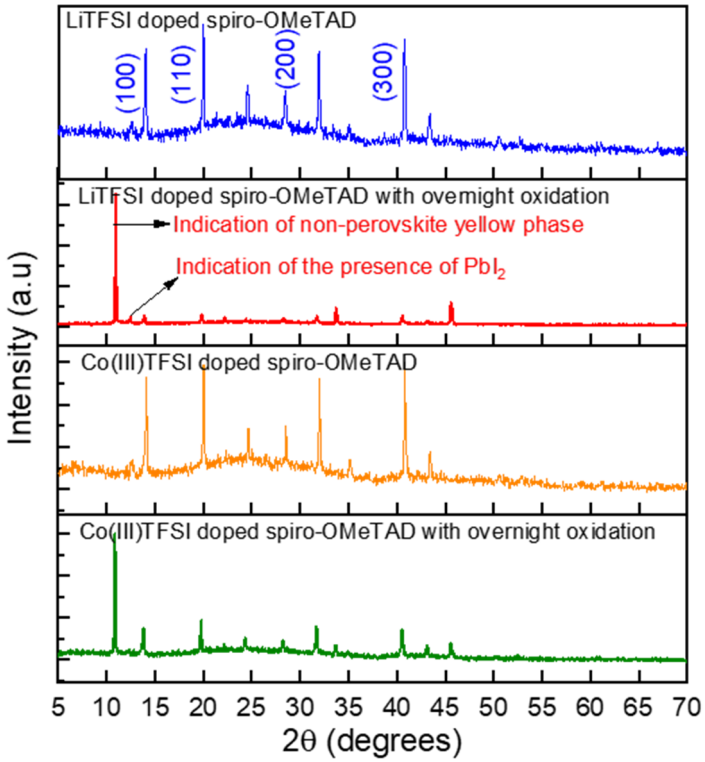

Figure 3. XRD patterns for perovskite/LiTFSI-doped spiro-OMeTAD and perovskite/Co(III)TFSI co-doped spiro-OMeTAD for different oxidation conditions.

The contact angles for LiTFSI-doped spiro-OMeTAD and Co(III)TFSI co-doped spiro-OMeTAD deposited on glass substrates with different oxidation conditions are obtained using diiodomethane (DIM). In the case of the LiTFSI-doped spiro-OMeTAD film, the results in Figure 4 show that the contact angle reduces from 40.11° without oxidation to 31.60° with overnight oxidation. On the contrary, there is no significant variation in the contact angle of Co(III)TFSI co-doped spiro-OMeTAD regardless of overnight oxidation. The contact angles with and without overnight oxidation are 48.75° and 52.60°, respectively. Apparently, it can be inferred that Co-based dopants exhibit a more hydrophobic nature compared to their Li counterparts. The contact angle measurement is also an indication of the moisture stability of the corresponding perovskite solar cells. In continuation of the experiments investigating the structural degradation as observed in XRD and the hydrophobicity as illustrated through contact angle, the devices were further analyzed for their device stability by maximum power point (MPP) tracking, as shown in Figure 5. All the devices were unencapsulated and tested under continuous light irradiation (AM 1.5 G, 100 mWcm^{-2}) for 3000 min in a nitrogen-purged glovebox. The device stability test results are summarized in Table 3. When the stability analysis was performed on a device with pristine spiro-OMeTAD as an HTM, the device degraded rapidly due to the absence of dopants.

In the case of devices with LiTFSI-doped spiro-OMeTAD without overnight oxidation, the device retained 54.8% of the initial PCE, whereas only 38.5% of the initial PCE could be retained for such devices with overnight oxidation. This poor stability is related to the hygroscopic nature of LiTFSI. Hence, although overnight oxidation improves the hole extraction rate of LiTFSI-doped spiro-OMeTAD and the corresponding device efficiency, it negatively affects the device stability. On the other hand, perovskite solar cells with Co(III)TFSI co-doped spiro-OMeTAD without overnight oxidation could retain 90.0% of the initial PCE, while 68.5% of the initial PCE is retained in the case of overnight oxidation. This stability reduction for devices with the overnight oxidation of Co(III)TFSI co-doped spiro-OMeTAD is also attributed to the presence of the hygroscopic LiTFSI in the oxidation process, as shown in Equation (2). For devices without overnight oxidation, the presence

of LiTFSI does not affect the stability because the films are not exposed to air and the oxidation process is time-independent. Therefore, in terms of device stability, perovskite solar cells with Co(III)TFSI co-doped spiro-OMeTAD perform better than their LiTFSI-doped counterparts in both cases. Furthermore, it is noticed that the device stability decreases when subjected to overnight oxidation regardless of the dopant type. This rapid degradation in efficiency is detrimental to the device's lifetime and imposes a serious limitation on the resulting energy yields.

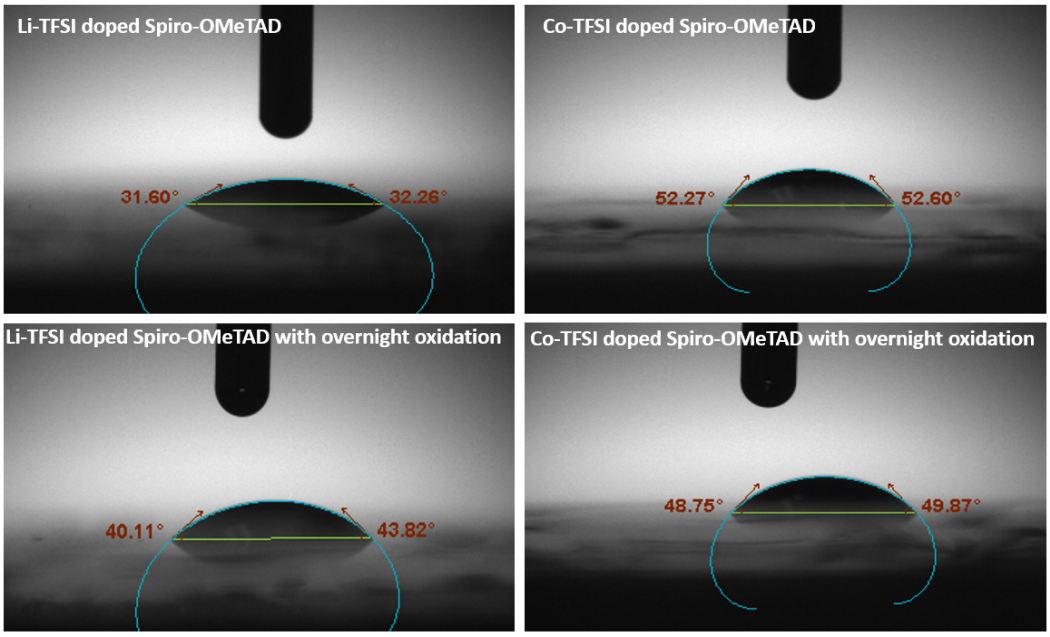

Figure 4. Contact angle measurements for LiTFSI-doped spiro-OMeTAD (31.60° and 40.11°, with and without overnight oxidation, respectively) and Co(III)TFSI co-doped spiro-OMeTAD (52.27° and 48.75°, with and without overnight oxidation, respectively).

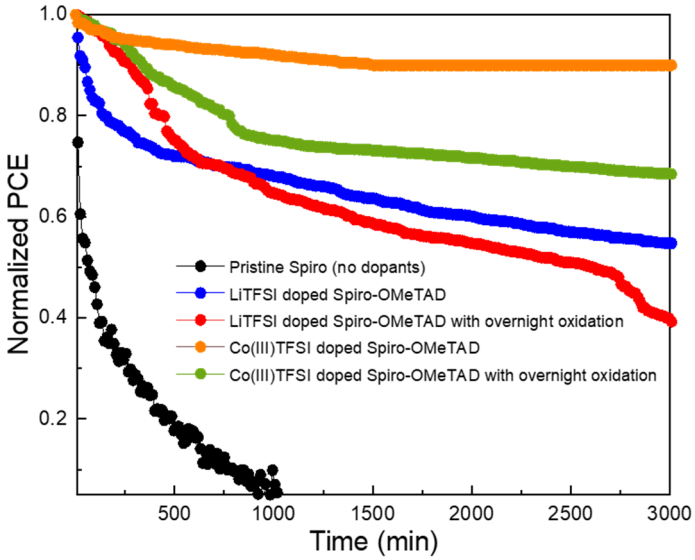

Figure 5. Stability analysis by the MPP tracking of perovskite solar cells with pristine spiro-OMeTAD, LiTFSI-doped spiro-OMeTAD, and Co(III)TFSI co-doped spiro-OMeTAD with and without overnight oxidation.

Table 3. Stability analysis for the unencapsulated perovskite solar cells. The power conversion efficiency (PCE) of perovskite solar cells with LiTFSI-doped spiro-OMeTAD and Co(III)TFSI co-doped spiro-OMeTAD with and without oxidation.

Device	PCE Retention (%)
PSC with pristine spiro-OMeTAD	0
PSC with LiTFSI-doped spiro-OMeTAD	54.8
PSC with LiTFSI-doped spiro-OMeTAD with overnight oxidation	38.5
PSC with Co(III)TFSI co-doped spiro-OMeTAD	90.0
PSC with Co(III)TFSI co-doped spiro-OMeTAD with overnight oxidation	68.5

4. Conclusions

In this work, we studied perovskite solar cells with LiTFSI-doped spiro-OMeTAD and Co(III)TFSI co-doped spiro-OMeTAD with and without overnight oxidation. In terms of the device properties, the efficiency of the perovskite solar cell with LiTFSI-doped spiro-OMeTAD was only 12.88% with overnight oxidation, compared to 9.18% without oxidation. Meanwhile, perovskite solar cells with Co(III)TFSI co-doped spiro-OMeTAD exhibited efficiencies of 17.58% with overnight oxidation and 17.6% without overnight oxidation, and the difference in efficiencies was negligible. This confirms that co-doping using cobalt complexes gives better device performance regardless of the presence of overnight oxidation. From the steady-state PL, time-resolved PL, and XRD results, it was found that using Co(III)TFSI co-doped spiro-OMeTAD results in superior material and electrical properties compared to LiTFSI-doped spiro-OMeTAD. Furthermore, it was found that overnight oxidation has a negative impact on long-term device stability for both LiTFSI-doped spiro-OMeTAD and Co(III)TFSI co-doped spiro-OMeTAD as HTMs. Co(III)TFSI co-doped spiro-OMeTAD without overnight oxidation demonstrated good stability, retaining 90% of the initial PCE after 3000 min of maximum power point tracking under 1-sun illumination. The results of the research demonstrate that doping spiro-OMeTAD with Co(III)TFSI does not require overnight oxidation due to its instant oxidation property. This study is useful to the perovskite community to simplify the process flow and fabrication time of perovskite solar cells based on Co(III)TFSI co-doped spiro-OMeTAD HTM.

Author Contributions: Conceptualization, L.N. and F.L.; data curation, L.N.; formal analysis, L.N. and F.L.; funding acquisition, A.G.A.; investigation, L.N.; methodology, F.L.; project administration, A.G.A. and F.L.; resources, A.G.A. and F.L.; supervision, A.G.A. and F.L.; validation, L.N.; writing—original draft, L.N.; writing—review and editing, A.G.A. and F.L. All authors have read and agreed to the published version of the manuscript.

Funding: This work is supported by the Solar Energy Research Institute of Singapore (SERIS), a research institute at the National University of Singapore (NUS). SERIS is supported by NUS, the National Research Foundation Singapore (NRF), the Energy Market Authority of Singapore (EMA), and the Singapore Economic Development Board (EDB).

Data Availability Statement: Not applicable.

Conflicts of Interest: The authors declare no conflict of interest. The funders had no role in the design of the study; in the collection, analysis, or interpretation of data; in the writing of the manuscript; or in the decision to publish the results.

References

1. Kojima, A.; Teshima, K.; Shirai, Y.; Miyasaka, T. Organometal halide perovskites as visible-light sensitizers for photovoltaic cells. *J. Am. Chem. Soc.* **2009**, *131*, 6050–6051. [CrossRef] [PubMed]
2. Best Research Efficiencies Chart for Perovskite Solar Cells, NREL. Available online: https://www.nrel.gov/pv/assets/pdfs/best-research-cell-efficiencies.20200925.pdf (accessed on 5 November 2022).
3. Kan, B.; Kan, Y.; Zuo, L.; Shi, X.; Gao, K. Recent progress on all-small molecule organic solar cells using small-molecule nonfullerene acceptors. *InfoMat* **2020**, *3*, 175–200. [CrossRef]
4. Gao, K.; Miao, J.; Xiao, L.; Deng, W.; Kan, Y.; Liang, T.; Peng, X. Multi-Length-Scale Morphologies Driven by Mixed Additives in Porphyrin-Based Organic Photovoltaics. *Adv. Mater.* **2016**, *28*, 4727–4733. [CrossRef] [PubMed]

5. Sun, Y.; Liu, T.; Kan, Y.; Gao, K.; Tang, B.; Li, Y. Flexible Organic Solar Cells: Progress and Challenges. *Small Sci.* **2021**, *1*, 2100001. [CrossRef]
6. Ma, R.; Zhou, K.; Sun, Y.; Liu, T.; Kan, Y.; Xiao, Y.; Peña, T.A.D.; Li, Y.; Zou, X.; Xing, Z.; et al. Achieving high efficiency and well-kept ductility in ternary all-polymer organic photovoltaic blends thanks to two well miscible donors. *Matter* **2022**, *5*, 725–734. [CrossRef]
7. Nian, L.; Gao, K.; Liu, F.; Kan, Y.; Jiang, X.; Liu, L.; Xie, Z.; Peng, X.; Russell, T.P.; Ma, Y. 11% Efficient ternary organic solar cells with high composition tolerance via integrated near-IR sensitization and interface engineering. *Adv. Mater.* **2016**, *28*, 8184–8190. [CrossRef]
8. Seong, S.S.; Seon, J.L.; Seok, S. Metal oxide charge transport layers for efficient and stable perovskite solar cells. *Adv. Func. Mater.* **2019**, *29*, 1900455. [CrossRef]
9. Jeon, N.J.; Na, H.; Jung, E.H.; Yang, T.-Y.; Lee, Y.G.; Kim, G.; Shin, H.-W. A fluorene-terminated hole-transporting material for highly efficient and stable perovskite solar cells. *Nat. Energy* **2018**, *3*, 682. [CrossRef]
10. Pham, H.D.; Escrig, L.G.; Feron, K.; Manzhos, S.; Albrecht, S.; Bolink, S.J.; Sonar, P. Boosting inverted perovskite solar cell performance by using 9,9-bis(4-diphenylaminophenyl)fluorene functionalized with triphenylamine as a dopant-free hole transporting material. *J. Mater. Chem. A* **2019**, *7*, 12507–12517. [CrossRef]
11. Pham, H.D.; Hayasake, K.; Kim, J.; Do, T.T.; Matsui, H.; Manzhos, S.; Feron, K.; Tokito, S.; Watson, T.; Tsoi, W.C.; et al. One step facile synthesis of a novel anthanthrone dye-based, dopant-free hole transporting material for efficient and stable perovskite solar cells. *J. Mater. Chem. C* **2018**, *6*, 3699–3708. [CrossRef]
12. Arora, N.; Dar, M.I.; Hinderhofer, A.; Pellet, N.; Schreiber, F.; Zakeeruddin, S.M.; Grätzel, M. Perovskite solar cells with CuSCN hole extraction layers yield stabilized efficiencies greater than 20%. *Science* **2018**, *358*, 768–771. [CrossRef]
13. Mali, S.S.; Patil, J.V.; Kim, H.; Luque, R.; Hong, C.K. Highly efficient thermally stable perovskite solar cells via Cs:NiOx/CuSCN double-inorganic hole extraction layer interface engineering. *Mater. Today* **2019**, *26*, 8–18. [CrossRef]
14. Ulzii, G.-T.; Matsushima, T.; Adachi, C. Mini-review of perovskite solar cells with spiro-OMeTAD hole transport layer: Recent progress and perspectives. *Energy Fuels* **2021**, *35*, 18915–18927. [CrossRef]
15. Nakka, L.; Cheng, Y.; Aberle, A.G.; Lin, F. Analytical review of spiro-OMeTAD hole transport materials: Paths toward stable and efficient perovskite solar cells. *Adv. Energy Sust. Res.* **2022**, *3*, 2200045. [CrossRef]
16. Abate, A.; Leijtens, T.; Pathak, S.; Teuscher, J.; Avolio, R.; Errico, M.E.; Kirkpatrik, J.; Ball, M.J.; Docampo, P.; McPherson, I.; et al. Lithium salts as "redox active" p-type dopants for organic semiconductors and their impact in solid-state dye-sensitized solar cells. *Phys. Chem. Chem. Phys.* **2013**, *15*, 2572–2579. [CrossRef]
17. Hawash, Z.; Ono, L.K.; Qi, Y. Recent advances in spiro-meotad hole transport material and its applications in organic–inorganic halide perovskite solar cells. *Adv. Mater. Interf.* **2017**, *5*, 1700623. [CrossRef]
18. Kato, Y.; Ono, L.K.; Lee, M.V.; Wang, S.; Raga, S.R.; Qi, Y. Silver iodide formation in methyl ammonium lead iodide perovskite solar cells with silver top electrodes. *Adv. Mater. Interf.* **2015**, *2*, 1500195. [CrossRef]
19. Hawash, Z.; Ono, L.K.; Raga, S.R.; Lee, M.V.; Qi, Y. Air-exposure induced dopant redistribution and energy level shifts in spin-coated spiro-MeOTAD films. *Chem. Mater.* **2015**, *27*, 562–569. [CrossRef]
20. Kim, G.W.; Kang, G.; Malekshahi Byranvand, M.; Lee, G.Y.; Park, T. Gradated mixed hole transport layer in a perovskite solar cell: Improving moisture stability and efficiency. *Appl. Mater. Interf.* **2017**, *9*, 27720–27726. [CrossRef]
21. Burschka, J.; Dualeh, A.; Kessler, F.; Baranoff, E.; Cevey-Ha, N.L.; Yi, C.; Nazeeruddin, M.; Graätzel, M. Tris (2-(1 H-pyrazol-1-yl) pyridine) cobalt (III) as p-type dopant for organic semiconductors and its application in highly efficient solid-state dye-sensitized solar cells. *J. Am. Chem. Soc.* **2011**, *133*, 18042–18045. [CrossRef]
22. Burschka, J.; Kessler, F.; Nazeeruddin, M.K.; Graätzel, M. Co (III) complexes as p-dopants in solid-state dye-sensitized solar cells. *Chem. Mater.* **2013**, *25*, 2986–2990. [CrossRef]
23. Noh, J.H.; Jeon, N.J.; Choi, Y.C.; Nazeeruddin, M.K.; Grätzel, M.; Seok, S.I. Nanostructured TiO2/CH3 NH3 PbI3 heterojunction solar cells employing spiro-OMeTAD/Co-complex as hole-transporting material. *J. Mater. Chem. A.* **2013**, *38*, 11842–11847. [CrossRef]
24. Song, Z.; Liu, J.; Wang, G.; Zuo, W.; Liao, C.; Mei, J. Understanding the Photovoltaic Performance of Perovskite–Spirobifluorene Solar Cells. *ChemPhysChem* **2017**, *18*, 3030–3038. [CrossRef] [PubMed]
25. Xi, H.; Tang, S.; Ma, X.; Chang, J.; Chen, D.; Lin, Z.; Zhang, C. Performance enhancement of planar heterojunction perovskite solar cells through tuning the doping properties of hole-transporting materials. *ACS Omega* **2017**, *2*, 326–336. [CrossRef] [PubMed]
26. Koh, T.M.; Dharani, S.; Li, H.; Prabhakar, R.R.; Mathews, N.; Grimsdale, A.C.; Mhaisalkar, S.G. Cobalt dopant with deep redox potential for organometal halide hybrid solar cells. *ChemSusChem* **2014**, *7*, 1909–1914. [CrossRef]
27. Payno, D.; Salado, M.; Andresini, M.; Gutiérrez-Moreno, D.; Huang, P.; Ciriaco, F.; Ahmad, S. Substituents interplay in piperidinyl-perylenediimide as dopant-free hole-selective layer for perovskite solar cells fabrication. *Emergent Mater.* **2014**, *5*, 977–985. [CrossRef]
28. Fang, H.H.; Adjokatse, S.; Shao, S.; Even, J.; Loi, M.A. Long-lived hot-carrier light emission and large blue shift in formamidinium tin triiodide perovskites. *Nat. Commun.* **2018**, *9*, 1–8. [CrossRef]

29. Sadhanala, A.; Deschler, F.; Thomas, T.H.; Dutton, S.E.; Goedel, K.C.; Hanusch, F.C.; Friend, R.H. Preparation of single-phase films of CH3NH3Pb(I1–xBrx)3 with sharp optical band edges. *J. Phys. Chem. Lett.* **2014**, *515*, 2501–2505. [CrossRef]
30. Jamal, M.S.; Shahahmadi, S.A.; Wadi, M.A.A.; Chelvanathan, P.; Asim, N.; Misran, H.; Akhtaruzzaman, M. Effect of defect density and energy level mismatch on the performance of perovskite solar cells by numerical simulation. *Optik* **2019**, *182*, 1204–1210. [CrossRef]
31. Xu, X.; Zheng, H.; Liu, G.; Zhu, L.; He, D.; Xu, S.; Pan, X. Elimination of Yellow Phase: An Effective Method to Achieve High Quality HC (NH2) 2PbI3-based Perovskite Films. *ChemSusChem* **2020**, *13*, 956–963. [CrossRef]